Magnetic Resonance in Medicine 44:758–765 (2000)

B_0-Fluctuation-Induced Temporal Variation in EPI Image Series Due to the Disturbance of Steady-State Free Precession

Xiaoli Zhao,[1] Jerzy Bodurka,[1,2] Andrzej Jesmanowicz,[1] and Shi-Jiang Li[1*]

Steady-state free precession (SSFP) can develop under a train of RF pulses, given the condition TR < T_2. SSFP in multi-shot imaging sequences has been well studied. It is shown here that serial single-shot echo-planar imaging (EPI) acquisition can also develop SSFP, and the SSFP can be disturbed by B_0 fluctuation, causing voxel-wise temporal variation. This SSFP disturbance is predominantly present in cerebrospinal fluid (CSF) regions due to the long T_2 value. By applying a sufficiently strong crusher gradient in the EPI pulse sequence, the temporal variation induced by SSFP disturbance can be suppressed due to diffusion. Evidence is provided to indicate that physiological motions such as cardiac pulsation and respiration could affect the voxel-wise time courses through the mechanism of SSFP disturbance. It is advised that if the disturbance is observed in serial EPI images, the crusher should be made stronger to eliminate the unwanted temporal variation. Magn Reson Med 44:758–765, 2000. © 2000 Wiley-Liss, Inc.

Key words: steady-state free precession; echo-planar imaging; B_0 fluctuation; crusher gradient, disturbance

Steady-state free precession (SSFP) (1–3) can be developed by a class of multi-shot fast imaging sequences that include fourier acqured steady-state technique (4), refocused fast low angle shot (FLASH) (5,6), and fast imaging with steady-state free precession (7). The train of the RF pulses in an SSFP sequence, under the condition TR $< T_2$, can form an echo signal S^- prior to an RF pulse that is due to the partial refocusing effect of the RF pulses (8). If echo signals are not spoiled, both the echo signal S^- and the post-pulse signal S^+ reach steady state and SSFP is established. Because of the existence of S^-, an SSFP sequence cannot provide an image with good T_1 contrast; rather, it provides a contrast dependent on T_1, T_2, TR, and RF flip angle (9). Spoiling S^- can significantly improve the image contrast (10). By randomly changing the phase of the RF pulses, SSFP can be disturbed, resulting in the fluctuation of both S^- and S^+ (10). This SSFP disturbance can introduce pronounced ghosts into the multi-shot image along the phase-encoding direction (10).

Although SSFP in multi-shot imaging sequences has been well studied, to our knowledge no experimental data have been reported to demonstrate the existence of SSFP during the acquisition of an EPI image series or its effects on voxel-wise time courses. A single-shot EPI pulse sequence (11,12), which is commonly used in fMRI studies, is repeated to acquire a series of EPI images. Under the condition TR $< T_2$, the train of imaging RF pulses would establish SSFP and the echo signal S^- would be present before each RF pulse. Consequently, the post-pulse signal S^+, which is the imaged signal, would be affected by the presence of S^-. If for any reason SSFP is disturbed, both S^- and S^+ would fluctuate, introducing variations into voxel-wise time courses.

In this study, we demonstrate that SSFP can indeed develop during serial EPI acquisition. In particular, we show that the magnetic field fluctuation can disturb the steady state of SSFP, introducing variations into the voxel-wise time courses. We also demonstrate that a sufficiently strong crusher gradient applied in the EPI pulse sequence, which enhances the effect of diffusion, can significantly suppress this kind of variation. A theoretical explanation is provided and is supported by computer simulation and phantom studies.

THEORY

Spin Evolution Under a Train of RF Pulses

A voxel is divided into a set of miniscule subvoxels. In each subvoxel, the field is considered to be homogeneous; thus, there is no intra-subvoxel dephasing. The evolution of the magnetization in the subvoxel located at position **r** will be analyzed.

Consider an imaging sequence with TR. The train of RF pulses of this sequence is applied along the x axis in the rotating coordinate frame. The flip angle is θ°. If the transverse and longitudinal magnetization in the subvoxel prior to the nth RF pulse are given, the transverse and longitudinal magnetization immediately after the nth RF pulse can be given, respectively, by

$$M_\perp^+(n) = M_\perp^-(n)\cos^2\left(\frac{\theta}{2}\right) + [M_\perp^-(n)]^*\sin^2\left(\frac{\theta}{2}\right) - iM_z^-(n)\sin(\theta), \quad [1]$$

$$M_z^+(n) = M_z^-(n)\cos(\theta) - \frac{i}{2}\{M_\perp^-(n) - [M_\perp^-(n)]^*\}\sin(\theta) \quad [2]$$

where $i = \sqrt{-1}$, $M_\perp^-(n) = M_x^-(n) + iM_y^-(n)$ and $M_z^-(n)$ are the respective transverse and longitudinal magnetization prior to the nth RF pulse (8). Due to T_1 relaxation, the

[1]Biophysics Research Institute, Medical College of Wisconsin, Milwaukee, Wisconsin.

[2]University School of Medical Sciences, Department of Biophysics, Bydgoszcz, Poland.

Grant sponsor: National Institute on Drug Abuse; Grant number: DA10214.

*Correspondence to: Shi-Jiang Li, Ph.D., Biophysics Research Institute, Medical College of Wisconsin, 8701 Watertown Plank Road, Milwaukee, WI 53226. E-mail: sjli@mcw.edu

Received 8 March 2000; revised 18 May 2000; accepted 3 July 2000.

longitudinal magnetization prior to the $(n+1)$th RF pulse is given by

$$M_z^-(n+1) = M_z^+(n)e^{-TR/T_1} + M_0(1 - e^{-TR/T_1}) \quad [3]$$

where M_0 is the initial longitudinal magnetization. The transverse magnetization prior to the $(n+1)$th RF pulse is given by

$$M_\perp^-(n+1) = M_\perp^+(n)e^{-TR/T_2}e^{i\Phi(r,n)} \quad [4]$$

where e^{-TR/T_2} is the T_2 decay factor and $\Phi(\mathbf{r},n)$ is the total phase accumulated during the nth TR interval.

According to the analysis by Zur et al. (10), the total accumulated phase $\Phi(\mathbf{r},n)$ can be given by

$$\Phi(\mathbf{r}, n) = \phi(\mathbf{r}) + \varphi(n) \quad [5]$$

where $\phi(\mathbf{r})$ is dependent on the position $\mathbf{r}$ of the subvoxel, and $\varphi(n)$ is independent of $\mathbf{r}$ but dependent on the index n.

The position-dependent phase $\phi(\mathbf{r})$ is induced by applied field gradients in the sequence and the static field inhomogeneity, given by

$$\phi(\mathbf{r}) = \int_0^{TR} \omega(\mathbf{r}, t)dt \quad [6]$$

where $\omega(\mathbf{r},t)$ is the resonance frequency offset at position $\mathbf{r}$ determined by both gradients and static field inhomogeneity. For a periodically repeated pulse sequence, $\omega(\mathbf{r},t)$ has the same temporal form for all TR intervals, so $\phi(\mathbf{r})$ does not depend on n.

The position-independent phase $\varphi(n)$ is the same for all subvoxels. It can be artificially introduced by changing the phase of RF pulses or by varying the frequency of the RF synthesizer (10). The fluctuation of magnetic flux density B_0 can also cause this kind of phase accumulation. Here B_0 fluctuation means that the magnetic field fluctuates in a large spatial scale so that within a voxel the B_0 change is the same for all subvoxels. When considering the effect of B_0 fluctuation only, the position-independent phase $\varphi(n)$ is given by

$$\varphi(n) = \int_{nTR}^{(n+1)TR} \gamma\Delta B_0(t)dt \quad [7]$$

where $\Delta B_0(t)$ represents B_0 fluctuation. Since $\Delta B_0(t)$ can have different temporal behaviors during different TR intervals, $\varphi(n)$ should depend on n.

Using Eqs. [1]–[4], the numerical solution of $M_\perp^-(n)$ and $M_\perp^-(n)$ in the subvoxel can be calculated iteratively for the given values of $\phi(\mathbf{r})$ and $\varphi(n)$. The pre-pulse echo signal $S^-(n)$ in a voxel is the sum of the $M_\perp^-(n)$ values of all its subvoxels. Similarly, the post-pulse signal $S^+(n)$ is the sum of all $M_\perp^-(n)$ values. If $\varphi(n)$ remains constant, the analytical solution of S^- and S^+ at steady state was given by Buxton et al. (13).

SSFP Disturbance Due to B_0 Fluctuation in Serial EPI Acquisition

Under a train of periodic RF pulses, when TR $< T_2$, both $S^-(n)$ and $S^+(n)$ reach steady state and SSFP develops. Although Eqs. [1]–[4] can be used to calculate the values of $S^-(n)$ and $S^+(n)$, they do not provide insight into the physical sources of these signals. Kaiser et al. (3) proposed a partition method that describes the physical sources of $S^-(n)$ and $S^+(n)$, showing that each RF pulse not only creates new transverse magnetization but also partially reverses the phases of the previous ones. The phase reversal allows dephased spins to approach an in-phase condition before a later RF pulse, and form the echo signal $S^-(n)$. Due to the existence of $S^-(n)$, signal $S^+(n)$ consists of not only the fresh FID signal tipped over by the most recent RF pulse, but also the component from the echo signal $S^-(n)$.

Kaiser et al. (3) considered only the position-dependent phase $\phi(\mathbf{r})$ in their analysis. Zur et al. (10) studied the relation between SSFP and position-independent phase $\varphi(n)$, demonstrating that the steady state of $S^-(n)$ and $S^+(n)$ is maintained only if the position-independent phase $\varphi(n)$ is a *linear* function of n. When $\varphi(n)$ is not linearly dependent on n, the echo signal $S^-(n)$ does not remain at a steady state but changes along with n. Since $S^+(n)$ contains a component from $S^-(n)$, the change of $S^-(n)$ also causes $S^+(n)$ to change, resulting in the disturbance of the steady state. Computer simulations by Zur et al. (10) showed that $S^+(n)$ fluctuated randomly when $\varphi(n)$ was a random function of n. Spoiling $S^-(n)$ can suppress the $S^+(n)$ fluctuation since the component from $S^-(n)$ is removed.

If B_0 fluctuation exists during serial EPI acquisition, the variation of position-independent phase $\varphi(n)$ is introduced as described by Eq. [7]. There are many sources of B_0 fluctuation. It has been reported that the chest motion related to respiration influences the magnetic field inside the field of view (FOV) (14,15). Other physical movements outside the FOV, such as swallowing and speaking, can also disturb the magnetic field (16). System instability and eddy currents (17) are other sources of B_0 changes. The complicated sources of B_0 fluctuation make $\varphi(n)$ change *nonlinearly* with n; according to the conclusion drawn by Zur et al. (10), SSFP is disturbed and $S^+(n)$ fluctuates. Since the $S^+(n)$ signal is imaged by a single RF pulse in EPI, $S^+(n)$ fluctuation will be reflected in the EPI image series. As a result, voxel-wise temporal variations are introduced by B_0 fluctuation. In human brain these temporal variations should be pronounced in the CSF-rich regions that have a long T_2 value; the condition TR $< T_2$, necessary for the development of SSFP, would thus be satisfied.

To suppress the $S^+(n)$ fluctuation, the $S^-(n)$ signal should be spoiled so that $S^+(n)$ does not contain the component from $S^-(n)$. Since the echo signal $S^-(n)$ is sensitive to spin diffusion, it can be attenuated by applying a gradient between RF pulses (18). Wu and Buxton (18) studied the diffusion effect of these gradients on the $S^-(n)$ and $S^+(n)$ signals in SSFP. They gave the analytical expression of the signal dependence on the diffusion coefficient, gradient length, and strength, and the TR, T_1, T_2, and flip

angle. According to their results, a sufficiently strong gradient can spoil the echo signal $S^-(n)$.

In a typical EPI pulse sequence, a crusher gradient is applied to crush the residual signal by enhancing the intravoxel dephasing. However, a crusher sufficient to dephase a signal may not be able to suppress the echo signal $S^-(n)$. As described before, the dephased signal can be rephased by the train of RF pulses and the echo signal $S^-(n)$ is formed. By increasing the duration of the crusher, it can function as a diffusion-enhancing gradient, and thus the echo signal can be suppressed. In our experiments, we used a 20 mT/m crusher of 10 msec duration to enhance the diffusion effect, and compared the results with the effects of a 1-msec crusher, which is only able to dephase the residual signal.

SIMULATION

To simulate $S^-(n)$ and $S^+(n)$ from a voxel in the presence of gradients and field inhomogeneity, the transverse magnetization of 500 subvoxels prior to and immediately after each RF pulse was calculated and summed, using Eqs. [1]–[4] iteratively. The $\phi(\mathbf{r})$ values in the 500 subvoxels were chosen to have uniform distribution from 0° to 360°. The $\Delta B_0(t)$ was assumed to be only a function of n and remained constant within a TR interval, so that $\varphi(n)$ can be expressed by

$$\phi(n) = \gamma \Delta B_0(n) TR \qquad [8]$$

rather than Eq. [7].

Three forms of $\Delta B_0(n)$ were chosen in the simulation. The first was $\Delta B_0(n) = 0$. The second was

$$\Delta B_0(n) = A \sin\left(\frac{2\pi n}{L}\right) \qquad [9]$$

where $A = 10$ nT, $L = 10$. In the third form, $\Delta B_0(n)$ fluctuated randomly in the range of ±10 nT. The other parameters were: $T_2 = 2.2$ sec, $T_1 = 3.75$ sec, flip angle $\theta = 45°$, TR = 0.2 sec and 1 sec. T_2 and T_1 values were chosen to be similar to those in the CSF.

In the simulation for $S^-(n)$ spoiling, the equation $M_\perp^-(n) = 0$ is used in place of Eq. [4] to guarantee that $S^-(n) = 0$.

EXPERIMENTS

EPI image series in both a phantom and humans were acquired using a 3T BIOSPEC 30/60 Bruker scanner, with a homemade local gradient coil and an endcapped birdcage RF head coil (19,20). Figure 1 shows the diagram of a single-shot gradient-recalled EPI sequence. The crusher was applied along the slice-selection direction. The strength of the crusher was 20 mT/m; two durations (1 msec and 10 msec) were used. Raw data were reconstructed online using in-house software and were further post-processed by the AFNI software package (21,22).

To introduce B_0 fluctuation, a phantom with two copper wire lines immersed in tap water was used as described in Ref. 23. B_0 fluctuation was generated by the oscillating electric current in the wires. The two parallel wires spaced

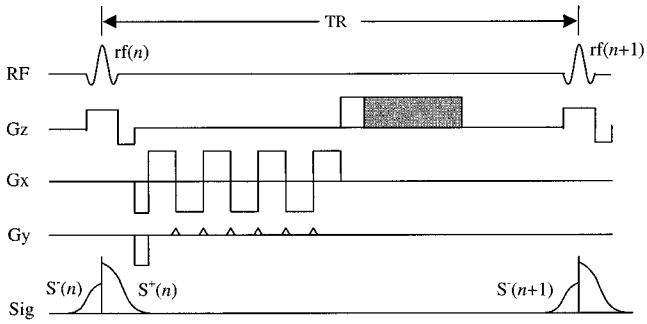

FIG. 1. Schematic diagram of a single-shot gradient-recalled EPI sequence for serial EPI acquisition. If TR < T_2, SSFP will be developed and two coherent signals, $S^-(n)$ and $S^+(n)$, will be formed prior to and immediately after the nth RF pulse. The SSFP can be spoiled by simply extending the duration of the crusher, as shown by the gray area.

5 cm apart were electrically connected and placed perpendicular to B_0. A sinusoidal electric current of frequency 1 Hz and amplitude 200 μA flowed through the two wires in opposite directions. The miniscule current ensured that for voxels away from the wires there was no detectable intravoxel dephasing due to the current. However, the current-induced B_0 changes were large enough to accumulate significant position-independent phases. For example, a constant 200 μA current changes B_0 by 3.2 nT for the voxel in the middle of the two wires. For TR = 200 msec, the accumulated phase is approximately 10°. For TR = 1 sec, it is approximately 50°.

With the sinusoidal current applied, serial EPI phantom images were acquired using 1- and 10-msec crushers. The scanning parameters were: $N = 150$, TR = 0.2 sec, TE = 27.2 msec, FOV = 12 cm, flip angle = 45°, slice thickness = 6 mm, image matrix = 64 × 64. For convenience in comparing results, the same flip angle (45°) was used as in the simulation.

Human experiments were performed on four subjects in the resting state. An axial slice across the two lateral ventricles was selected. Serial EPI images were acquired using 1- and 10-msec crushers. Two values of TR (0.2 sec and 1 sec) were used. The other scanning parameters were: $N = 150$, TE = 27.2 msec, FOV = 20 cm, flip angle = 45°, slice thickness = 6 mm, image matrix = 64 × 64.

In the Theory section we predicted that SSFP disturbance would be pronounced in CSF regions that have a long T_2 value. However, in the literature concerning CSF T_2 measurements there are considerable discrepancies in the reported T_2 values—ranging from several hundred msec to more than 2 sec (reviewed by Condon et al. (24)). We therefore performed the measurements of CSF T_2 ourselves. The measurements were performed on three subjects. A sagittal slice across the lateral ventricle was selected. Single-shot spin-echo EPI images were acquired with TE = 55, 150, 300, 600, 1000, 1500, 2000, 2500, and 3000 msec. The time interval between two image acquisitions was greater than 15 sec to avoid T_1 saturation. The other scanning parameters were: FOV = 20 cm, slice thickness = 4 mm, image matrix = 64 × 64. T_2 values were calculated by averaging the signal intensities of four adjacent voxels in the lateral ventricle for each

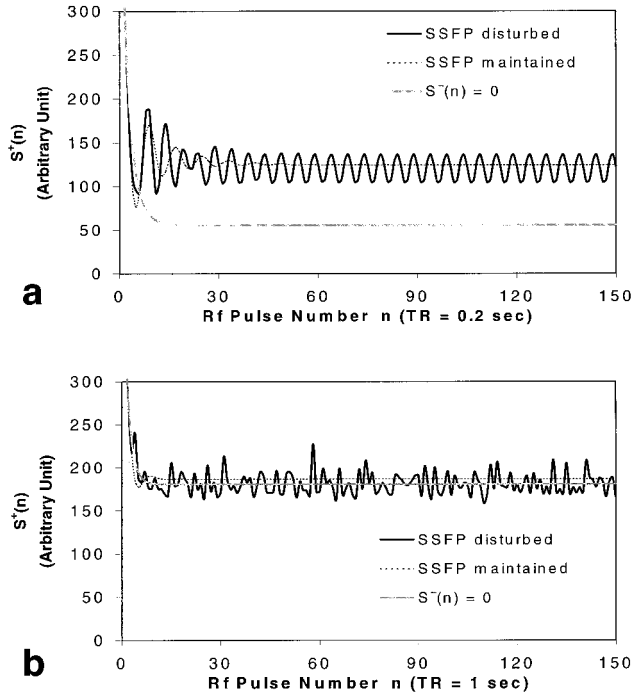

FIG. 2. Simulation of time courses under different forms of $\Delta B_0(n)$. **a:** $\Delta B_0(n)$ is a sinusoidal function of n or remains at zero. TR = 0.2 sec. **b:** $\Delta B_0(n)$ is a random function of n or remains at zero. TR = 1 sec. When $\Delta B_0(n) = 0$, SSFP is established and maintained (broken lines). When $\Delta B_0(n)$ changes sinusoidally or randomly with n, SSFP is disturbed (dark solid lines). When $S^-(n) = 0$, the temporal fluctuations due to SSFP disturbance are suppressed (light solid lines).

TE and then performing least-squares fits based on the mono-exponential T_2 decay model.

RESULTS

Simulation Results

The simulation results are shown in Fig. 2. Figure 2a shows the $S^+(n)$ time courses at TR = 0.2 sec when $\Delta B_0(n)$ remained at zero or oscillated sinusoidally. For $\Delta B_0(n) = 0$, $S^+(n)$ reached steady state after the initial non-equilibrium and SSFP was established and maintained. When $\Delta B_0(n)$ oscillated, SSFP was disturbed and $S^+(n)$ changed sinusoidally around the steady-state level. When $S^-(n) = 0$, the $S^+(n)$ oscillation was suppressed. Figure 2b shows the $S^+(n)$ time courses at TR = 1 sec for randomly changing $\Delta B_0(n)$. The fluctuation was suppressed when $S^-(n) = 0$.

It is noted that at TR = 0.2 sec, the baselines of the SSFP-disturbed and SSFP-maintained time courses are much higher than the time course with $S^-(n) = 0$ (Fig. 2a); at TR = 1 sec the baseline difference is smaller (Fig. 2b). This is because the baseline difference is dependent on the TR and RF pulse flip angle, as analyzed by Wu and Buxton (18). A smaller TR value results in a larger baseline difference. For a given TR, the baseline difference is increased by a relatively large RF flip angle. We chose a flip angle (45°) larger than the Ernst angle for TR = 0.2 sec to enhance the baseline difference for clearer demonstration.

Phantom Results

Figures 3 and 4 summarize the results of phantom exper-

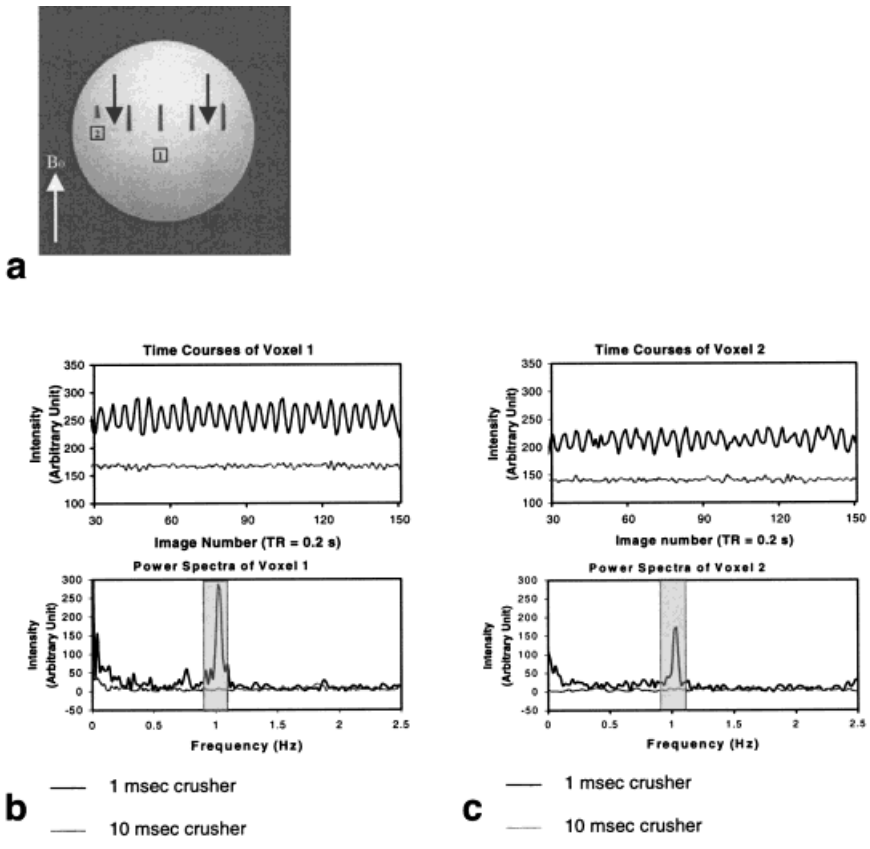

FIG. 3. Results of phantom experiments. **a:** The image of the studied slice. Two arrows indicate the locations of the wires. Box 1 and box 2 indicate the location of the two representative voxels. **b:** Time courses and power spectra of the central voxel of box 1. **c:** Time courses and power spectra of the central voxel of box 2.

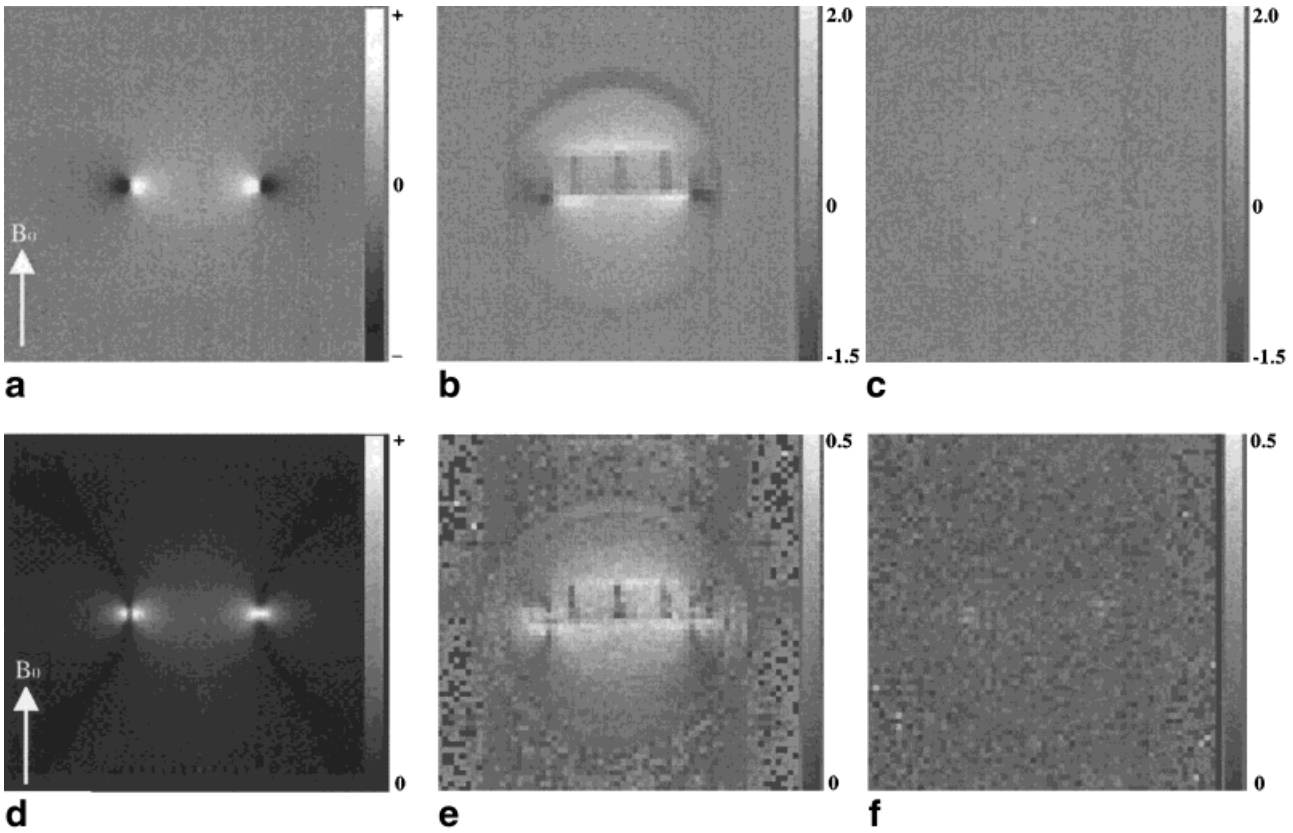

FIG. 4. Results of phantom experiments. **a:** Electric-current-induced ΔB_0 map at a representative moment. **b, c:** Functional intensity maps (see text) with 1-msec (**b**) and 10-msec (**c**) crushers. **d:** Electric-current-induced $|\Delta B_0|$ map at a a representative moment. **e, f:** Spectral images of the frequency components around 1 Hz, with 1-msec (**e**) and 10-msec (**f**) crushers.

iments. Figure 3a shows the image of the phantom. The two arrows indicate the locations of the axial cross-sections of the wires, which were supported by a plastic frame (seen as the dark structure). B_0 was parallel to the imaging plane, as marked. Two voxels were selected as representatives; their time courses and power spectra are shown in Fig. 3b and c. With a 1-msec crusher the time course oscillations were pronounced, while with a 10-msec crusher the oscillations were suppressed. The baseline of a time course with the 1-msec crusher is higher. These results are consistent with the simulations, suggesting that SSFP existed in the serial EPI acquisitions and the voxel-wise temporal oscillations were induced by the disturbance of SSFP. With the 1-msec crusher, the power spectrum has a distinct peak located around 1 Hz, the frequency of the sinusoidal electric current. The peak was suppressed when the 10-msec crusher was applied. These results indicate that SSFP disturbance was caused by the oscillating electric current.

Figure 4a shows a simulated ΔB_0 map induced by current. Figure 4b and c shows the respective functional intensity maps with the 1- and 10-msec crushers, using the time courses of voxel 1 (Fig. 3b) as references. The functional intensity of a voxel is defined as

$$\alpha = \rho|\mathbf{x}|/|\mathbf{r}| \qquad [10]$$

where ρ is the correlation coefficient, $\mathbf{x}$ is the time course in the voxel, and $\mathbf{r}$ is the reference time course (25). The functional intensity measures both the similarity and fluctuation intensity of a time course relative to the reference time course.

Figure 4d is a simulated current-induced $|\Delta B_0|$ map. Figure 4e (1-msec crusher) and f (10-msec crusher) were formed by integrating the spectral data for each voxel in the range of 0.9–1.1 Hz, as indicated by the gray bands in Fig. 3b and c. The integral result in each voxel was divided by the total area under the spectrum for normalization.

With the 1-msec crusher, the pattern of the functional intensity map (Fig. 4b) is similar to the ΔB_0 map (Fig. 4a), and the spectral image (Fig. 4e) is similar to the $|\Delta B_0|$ map (Fig. 4d). These similarities disappeared when the 10-msec crusher was applied. These results strongly support that the voxel-wise temporal oscillations due to SSFP disturbance were caused by B_0 changes, which were suppressed by applying a sufficiently strong crusher.

Human Results

The results of the CSF T_2 measurements are listed in Table 1. The T_2 values for the three subjects are 1802, 1931, and

Table 1
The Measured CSF T_2 Values for Three Subjects

Subject	T_2 (msec)
1	1802 ± 63
2	1931 ± 77
3	1841 ± 99

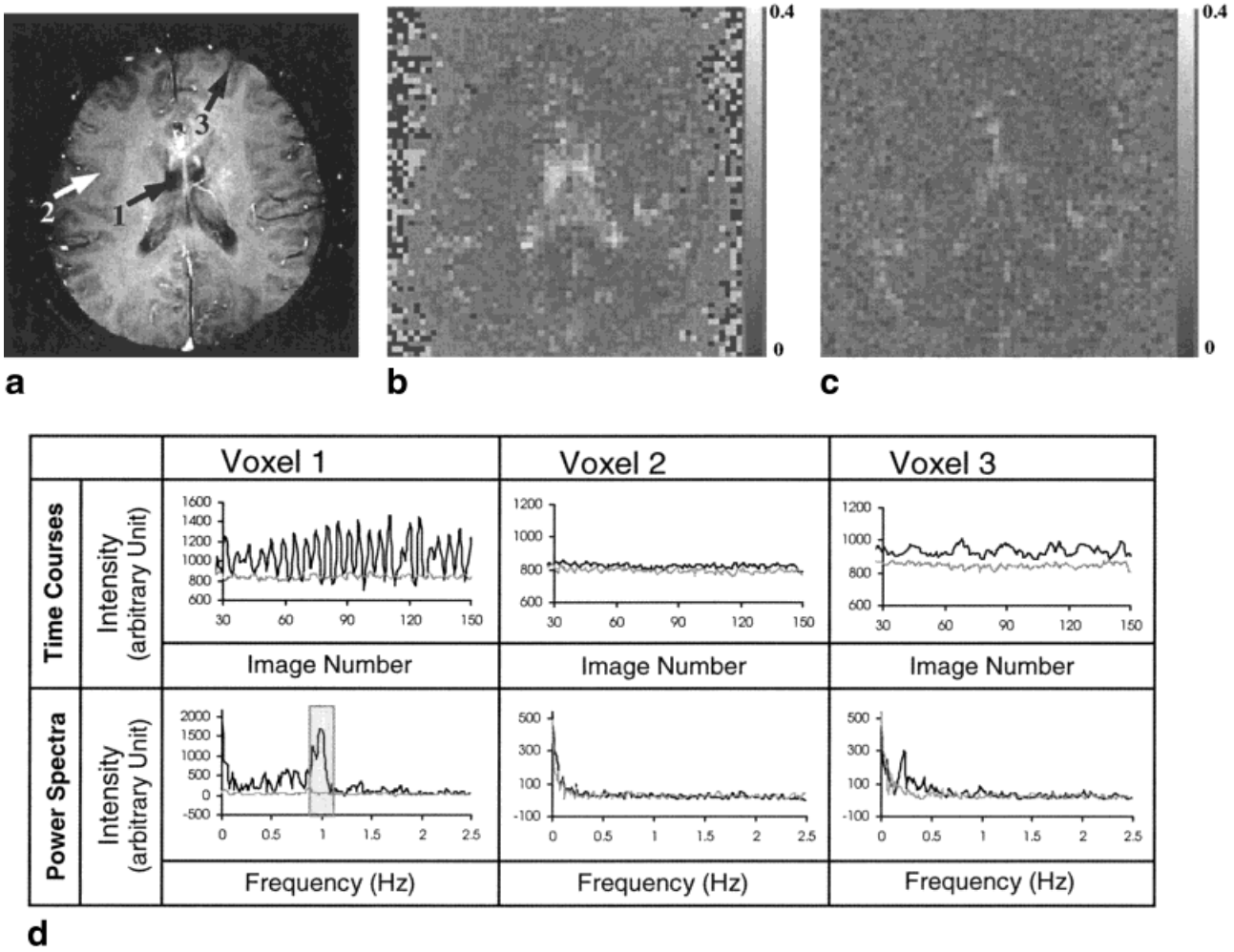

FIG. 5. Results of human experiments. TR = 0.2 sec. **a:** Anatomic image of the axial slice across lateral ventricles. Arrows indicate the location of the three representative voxels. **b, c:** Spectral images from the frequency components related to cardiac pulsation, with 1-msec (**b**) and 10-msec (**c**) crushers. **d:** Time courses and power spectra of the three representative voxels. Darker lines: with 1-msec crusher. Lighter lines: with 10-msec crusher.

1841 msec. The differences may be due to the partial volume effect (26).

For the SSFP disturbance studies, the results obtained from the four human subjects were similar. Figures 5 and 6 show the results from one of the subjects. Three representative voxels were selected (Fig. 5a): one in CSF (voxel 1), one in gray matter (voxel 2), and one at the edge of gray matter (voxel 3). With TR = 0.2 sec their time courses and power spectra are shown in Fig. 5d. For a 1-msec crusher, the temporal characteristics and the spectral properties of these three voxels are different. The temporal fluctuation is much more intense in voxel 1 than in voxel 2. The fluctuation intensity of voxel 3 is between that of voxels 1 and 2. The spectrum of voxel 1 has a peak located around 1 Hz, which is the frequency of cardiac pulsation. The spectrum of voxel 3 has a small peak around 0.2 Hz, the frequency of respiration. These differences are attributed to the T_2 values. The T_2 of CSF is approximately 1.8 sec as measured, whereas the T_2 of gray matter is approximately 0.1 sec (27). Since TR = 0.2 sec is less than the T_2 of CSF and larger than that of gray matter, the SSFP was disturbed only in the voxels containing CSF, where the condition $TR < T_2$ for developing SSFP is satisfied. Among the three representatives, voxel 1 contained the largest amount of CSF, so it showed the largest fluctuation. Voxel 3 mainly contained gray matter, but CSF was also present; therefore, the fluctuation still existed due to the partial volume effect, but was smaller than voxel 1. When a 10-msec crusher was applied, the temporal fluctuations and spectral peaks in voxel 1 and 3 were suppressed. The global effects of cardiac pulsation on CSF and on white and gray matter are shown in Fig. 5b (1-msec crusher) and c (10-msec crusher). These images were formed by the same method as in Fig. 4e and f, but the integral range was 0.75–1.25 Hz, as indicated by the gray band in Fig. 5d. The lateral ventricles containing CSF are defined better in Fig. 5b than in Fig. 5c, indicating that the 10-msec crusher significantly suppressed the cardiac pulsation-related fluctuations in CSF.

In the spectral domain, with the 1-msec crusher (in addition to the cardiac pulsation and respiration frequencies) other frequencies also have higher intensities than with the 10-msec crusher (spectra of voxel 1 and voxel 3 in

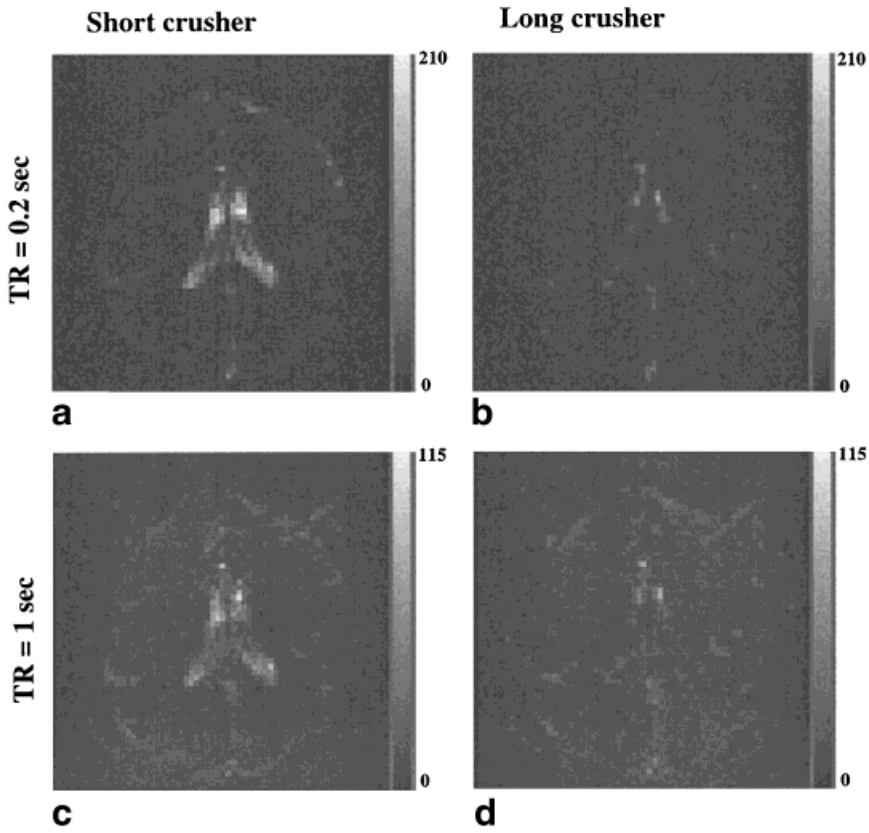

FIG. 6. Images of standard deviation for human experiments. **a, b:** TR = 0.2 sec, with 1-msec (**a**) and 10-msec (**b**) crushers. **c, d:** TR = 1 sec, with 1-msec (**c**) and 10-msec (**d**) crushers.

Fig. 5d). This is because other sources affecting B_0 also contributed to the signal fluctuation. The overall effects of B_0 fluctuation on the voxel-wise time courses are shown in the standard deviation images (Fig. 6). The lateral ventricles have much clearer shapes with the 1-msec crusher than with the 10-msec one, showing that the temporal variations due to SSFP disturbance existed mainly in the CSF region, even when TR was as long as 1 sec.

DISCUSSION

In fMRI studies blood oxygenation level-dependent (BOLD) signal is only about 5%, and reducing artificial noise is of paramount importance for determination of neuronal activity. The present study demonstrates that a tiny B_0-fluctuation can introduce significant noise into a voxel-wise time course due to SSFP disturbance. A B_0 variation of 10 nT causes a phase variation of approximately 150° for TR = 1 sec, and the noise induced is huge, as shown by the simulation in Fig. 2. Such a miniscule phase variation can have various uncontrolled sources, such as physiological motions; thus, the noise induced by SSFP disturbance could predominate in the CSF-rich gray matter regions due to the partial volume effect. Because B_0-fluctuation is global, the SSFP-disturbance-induced noise is coherent among the time courses. The coherence of the noise could interfere with the cross-correlation calculation for functional mapping when choosing a voxel-wise time course as a reference, and could also hinder the study of spontaneous low-frequency physiological fluctuations of neuronal origin (28). In the studies of early response of BOLD signal (29), the subtle differences in the onset of activation need to be detected with short TR. The SSFP disturbance could also be problematic. Therefore, it is important to understand the physical mechanism of the SSFP disturbance, and to know how to eliminate it if it presents.

In a typical EPI sequence, a crusher that is sufficient for intravoxel dephasing may be too weak to spoil the echo signal $S^-(n)$ by diffusion. In this case, the EPI pulse sequence should be modified to increase the length or strength of the crusher to suppress the unwanted variations. Using a large crusher may set up more eddy currents, which can affect the signal of the next image. However, by comparing the voxel time courses from gray and white matter using either a 1-msec or 10-msec crusher, we did not observe any difference (voxel 2 in Fig. 5d). This may be due to the fact that our gradient system is eddy current compensated. Furthermore, in a typical multi-slice fMRI study, the TR is long enough to naturally eliminate the effect of the eddy current induced by the crusher.

SSFP disturbance is more pronounced in CSF-rich regions due to its long T_2 value. However, the misleading underestimations of the CSF T_2 value (mostly around 200–300 msec) in some publications (24) could diminish the significance of the present study, because the TR used by a typical fMRI study is in the range of several hundred milliseconds to several seconds, which is larger than the published underestimated T_2 values. We therefore performed the T_2 measurement ourselves using the single-shot spin-echo EPI method. Underestimations of T_2 value

were mainly due to the misuse of short TE, and the imperfect (nonrectangular) slice profile of the refocusing pulses in a multiple spin-echo sequence (24,30,31). Insufficient sampling points, B_1 variation, and B_0 inhomogeneity can further deteriorate the underestimation (30–32). Our measurement of CSF T_2 is about 1.8 sec. Even this result might underestimate the CSF T_2 due to the partial volume effect, as studied by Cheng (26). He found that significant improvement of CSF T_2 measurement could be achieved by using a biexponential model to avoid the partial volume effect. The long CSF T_2 makes it highly probable the SSFP disturbance will present in a typical fMRI study, adding noise to the time courses in CSF-rich regions.

ACKNOWLEDGMENTS

This work was supported in part by grant DA10214 from the National Institute on Drug Abuse (to S.-J.L.). The authors thank Ms. Hollis Brunner for editorial assistance.

REFERENCES

1. Carr HY. Steady-state free precession in nuclear magnetic resonance. Phys Rev 1958;112:1693–1701.
2. Freeman R, Hill HDW. Phase and intensity anomalies in Fourier transform NMR. J Magn Reson 1971;4:366–383.
3. Kaiser R, Bartholdi E, Ernst RR. Diffusion and field-gradient effects in NMR Fourier spectroscopy. J Chem Phys 1974;60:2966–2979.
4. Gyngell ML, Palmer ND, Eastwood LM. The application of steady-state free precession (SFP) in 2D-FT MR imaging. In: Proceedings of the 5th Annual Meeting of SMRM, Montreal, Canada, 1986. p 666–667.
5. Darrasse L, Mao L, Saint-Jalmes H. Steady-state management in fast low-angle imaging. In: Proceedings of the 5th Annual Meeting of SMRM, Montreal, Canada, 1986. p 944–955.
6. Frahm J, Hanicke W, Merboldt K-D. Transverse coherence in rapid FLASH NMR imaging. J Magn Reson 1987;72:307–314.
7. Weber H, Purdy D, Deimling M, Oppelt A. Contrast behavior of the fast imaging sequences FLASH and FISP: results from synthetic images. In: Proceedings of the 5th Annual Meeting of SMRM, Montreal, Canada, 1986. p 957–958.
8. Woessner DE. Effects of diffusion in nuclear magnetic resonance spin-echo experiments. J Chem Phys 1961;34:2057–2061.
9. Zur Y, Stokar S, Bendel P. An analysis of fast imaging sequences with steady-state transverse magnetization refocusing. Magn Reson Med 1988;6:175–193.
10. Zur Y, Wood ML, Neuringer LJ. Spoiling of transverse magnetization in steady-state sequences. Magn Reson Med 1991;21:251–263.
11. Mansfield P. Multi-planar image formation using NMR spin echoes. J Phys C: Solid State Phys 1977;10:L55–L58.
12. Mansfield P, Pykett IL. Biological and medical imaging by NMR. J Magn Reson 1978;29:355–373.
13. Buxton RB, Fisel CR, Chien D, Brady TJ. Signal intensity in fast NMR imaging with short repetition times. J Magn Reson 1989;83:576–585.
14. Noll DC, Schneider W. Theory, simulation, and compensation of physiological motion artifacts in functional MRI. In: Proceedings of the 1st Annual IEEE Conference on Image Processing, Austin, Texas, 1994. p 40–44.
15. Noll DC, Schneider W. Respiration artifacts in functional brain imaging: sources of signal variation and compensation strategies. In: Proceedings of the 12th Annual Meeting of SMRM, New York, 1993. p 1407.
16. Birn RM, Bandettini PA, Cox RW, Jesmanowicz A, Shaker R. Magnetic field changes in the human brain due to swallowing or speaking. Magn Reson Med 1998;40:55–60.
17. Ahn CB, Cho ZH. Analysis of eddy-current in nuclear magnetic resonance imaging. Magn Reson Med 1991;17:149–163.
18. Wu EX, Buxton RB. Effect of diffusion on the steady-state magnetization with pulsed field gradients. J Magn Reson 1990;90:243–253.
19. Wong EC, Bandettini PA, Hyde JS. Echo-planar imaging of the human brain using a three axis local gradient coil. In: Proceedings of the 11th Annual Meeting of SMRM, Berlin, Germany, 1992. p 105.
20. Wong EC, Tan G, Hyde JS. A quadrature transmit-receive endcapped birdcage coil for imaging of the human head at 125 MHz. In: Proceedings of the 12th Annual Meeting of SMRM, New York, 1993. p 1344.
21. Cox RW. AFNI: software for analysis and visualization of functional magnetic resonance neuroimages. Comput Biomed Res 1996;29:162–173.
22. Cox RW, Hyde JS. Software tools for analysis and visualization of fMRI data. NMR Biomed 1997;10:171–178.
23. Bodurka J, Jesmanowicz A, Hyde JS, Xu H, Estkowski L, Li S-J. Current-induced magnetic resonance phase imaging. J Magn Reson 1999;137:265–271.
24. Condon B, Patterson J, Jenkins A, Wyper D, Hadley D, Grant R, Rowan J, Teasdale G. MR relaxation times of cerebrospinal fluid. J Comput Assist Tomogr 1987;11:203–207.
25. Cox RW, Jesmanowicz A, Hyde JS. Real-time functional magnetic resonance imaging. Magn Reson Med 1995;33:230–236.
26. Cheng KH. In vivo tissue characterization of human brain by chi squares parameter maps: multiparameter proton T_2-relaxation analysis. Magn Reson Imaging 1994;12:1099–1109.
27. Schad LR, Brix G, Zuna I, Harle W, Lorenz WJ, Semmler W. Multiexponential proton spin-spin relaxation in MR imaging of human brain tumors. J Comput Assist Tomogr 1989;13:577–587.
28. Biswal B, Yetkin FZ, Haughton VM, Hyde JS. Functional connectivity in motor cortex of resting human brain using echo-planar MRI. Magn Reson Med 1995;34:537–541.
29. Hu X, Le TH, Ugurbil K. Evaluation of the early response in fMRI in individual subjects using short stimulus duration. Magn Reson Med 1997;37:877–884.
30. Poon CS, Henkelman RM. Practical T2 quantitation for clinical applications. J Magn Reson Imaging 1992;2:541–553.
31. Majumdar S, Orphanoudakis SC, Gmitro A, O'Donnel M, Gore JC. Error in the measurements of T_2 using multiple-echo MRI techniques: 1. Effect of radiofrequency pulse imperfections. Magn Reson Med 1986;3:397–417.
32. Majumdar S, Orphanoudakis SC, Gmitro A, O'Donnel M, Gore JC. Error in the measurements of T2 using multiple-echo MRI techniques: 2. Effects of static field inhomogeneity. Magn Reson Med 1986;3:562–574.